JACS
JOURNAL OF THE AMERICAN CHEMICAL SOCIETY
Article
pubs.acs.org/JACS

Defining the Structural Basis for Allosteric Product Release from *E. coli* Dihydrofolate Reductase Using NMR Relaxation Dispersion

David Oyen, R. Bryn Fenwick, Phillip C. Aoto,† Robyn L. Stanfield, Ian A. Wilson, H. Jane Dyson, and Peter E. Wright*

Department of Integrative Structural and Computational Biology and Skaggs Institute for Chemical Biology, The Scripps Research Institute, 10550 North Torrey Pines Road, La Jolla, California 92037, United States

Supporting Information

ABSTRACT: The rate-determining step in the catalytic cycle of *E. coli* dihydrofolate reductase is tetrahydrofolate (THF) product release, which can occur via an allosteric or an intrinsic pathway. The allosteric pathway, which becomes accessible when the reduced cofactor NADPH is bound, involves transient sampling of a higher energy conformational state, greatly increasing the product dissociation rate as compared to the intrinsic pathway that obtains when NADPH is absent. Although the kinetics of this process are known, the enzyme structure and the THF product conformation in the transiently formed excited state remain elusive. Here, we use side-chain proton NMR relaxation dispersion measurements, X-ray crystallography, and structure-based chemical shift predictions to explore the structural basis of allosteric product release. In the excited state of the E:THF:NADPH product release complex, the reduced nicotinamide ring of the cofactor transiently enters the active site where it displaces the pterin ring of the THF product. The *p*-aminobenzoyl-L-glutamate tail of THF remains weakly bound in a widened binding cleft. Thus, through transient entry of the nicotinamide ring into the active site, the NADPH cofactor remodels the enzyme structure and the conformation of the THF to form a weakly populated excited state that is poised for rapid product release.

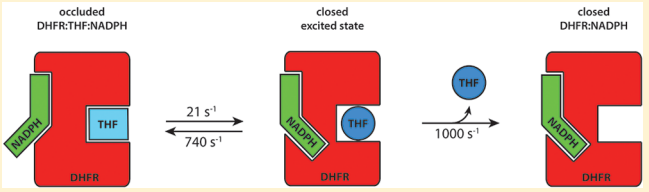

INTRODUCTION

Although much can be learned from static structures of proteins, their dynamic motions are intimately involved in their functions. The conformational landscapes of enzymes frequently include sparsely populated excited states that have direct relevance to the progression of catalysis. A number of recent studies have implicated polypeptide chain dynamics and low-population excited states in allostery, ligand exchange kinetics, and even the chemical step of a number of enzymes.[1−12] NMR is an especially powerful method for probing the dynamics of enzymes over a wide range of time scales and for characterizing their excited states.[13,14] Several NMR experiments provide information on conformational fluctuations occurring on the microsecond−millisecond time scale, including Carr−Purcell−Meiboom−Gill (CPMG) relaxation dispersion,[15] rotating-frame relaxation ($R_{1\rho}$),[16] and chemical exchange saturation transfer (CEST) or dark state exchange saturation transfer (DEST).[17,18] For a given nucleus, analysis of these data typically yields the exchange rate, the populations of the different states involved, and the chemical shift difference between the ground and excited states. The chemical shift differences provide insights into the conformational changes that occur in the transition to the excited state and can be used to generate structural models.[19]

Our understanding of the role of protein dynamics in enzyme catalysis has benefited greatly from extensive studies using the *E. coli* enzyme dihydrofolate reductase (DHFR) as a model system.[4,20,21] DHFR catalyzes the NADPH-dependent reduction of dihydrofolate (substrate, DHF) to tetrahydrofolate (product, THF), for which the rate-limiting step is product release[22] (Figure 1). Under saturating ligand concentrations, *E. coli* DHFR cycles through five intermediate states while switching between closed and occluded conformations of the loops adjacent to the active site.[4,23] NMR relaxation dispersion measurements for each of these five DHFR complexes revealed exchange with one or more minor populated states that resemble the conformation of the previous and/or next intermediate state in the catalytic cycle.[4]

Recent efforts to characterize the dynamics of DHFR have focused on a quantitative description of the role of protein dynamics in promoting product release.[12] An integrated approach using stopped-flow fluorescence and backbone amide ^{1}H and ^{15}N CPMG relaxation dispersion measurements showed that release of THF occurs via intrinsic and allosteric pathways.[12] Product release via the intrinsic pathway is slow and involves spontaneous dissociation of THF from any of the product-bound intermediates in the DHFR catalytic cycle. In contrast, product release via the allosteric pathway is rapid and involves release of THF from a weakly populated excited state that is formed by transient entry of the NADPH nicotinamide group into the catalytic site of the E:THF:NADPH complex

Received: June 8, 2017
Published: July 24, 2017

DOI: 10.1021/jacs.7b05958
J. Am. Chem. Soc. 2017, 139, 11233−11240

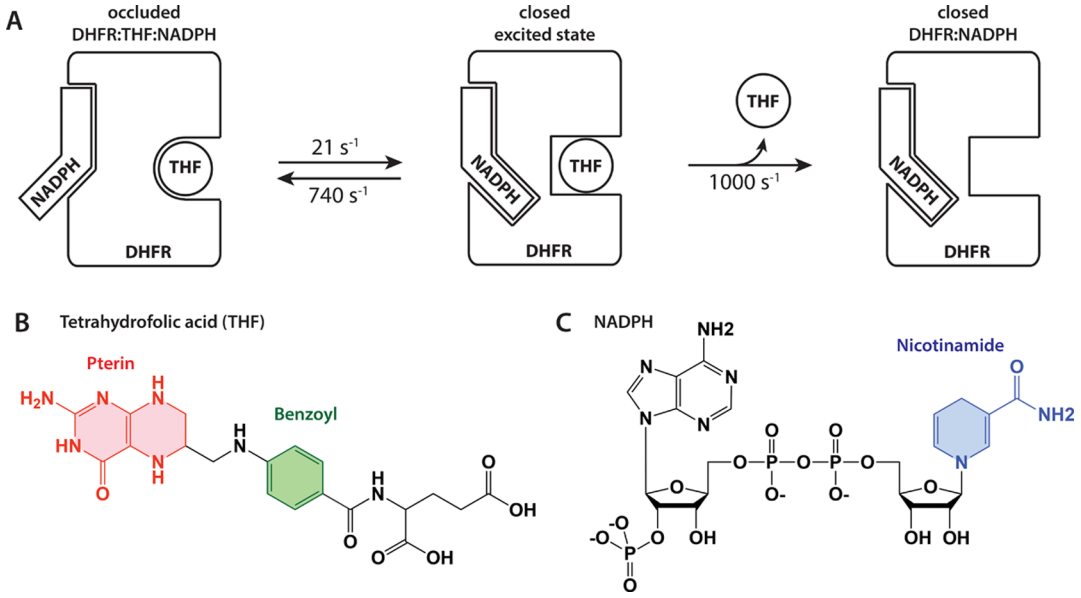

Figure 1. (A) Schematic illustration of the allosteric pathway for product release from DHFR. The rate constants are for the L28F mutant.[12] (B) Structure of the product tetrahydrofolate, with the pterin and benzoyl rings highlighted. (C) Structure of the reduced cofactor NADPH, highlighting the nicotinamide ring.

(shown schematically in Figure 1). Chemical shift differences derived from CPMG relaxation dispersion measurements indicate that the backbone conformation of the E:THF:NADPH excited state closely resembles that of the closed E:NADPH complex of DHFR.[12] Paradoxically, indirect evidence from binding kinetics, simulations, and concentration-independent relaxation dispersion suggests that THF remains bound in the excited state.[4,12]

Here, we use methyl proton relaxation dispersion to characterize the excited state of the E:THF:NADPH complex to obtain insights into the structural basis for allosteric release of THF product. Proton chemical shifts of side chains within the DHFR active site are highly sensitive to the location of the product because of the ring currents[24] associated with the aromatic motifs (the pterin group and the benzoyl ring in the *p*-aminobenzoyl-L-glutamate (pABG) tail, Figure 1B) of THF. If one or both of the two aromatic rings of the product changes position between the ground and excited states, then it is expected that the methyl proton chemical shifts of neighboring aliphatic amino acids will also change significantly. In addition, the ^{15}N chemical shift of Ala6 is strongly influenced by hydrogen-bonding interactions between the pterin ring and the backbone carbonyl of Ile5 and is therefore a sensitive probe of THF interactions.[25] Because the wild-type and Leu28Phe (L28F) mutant enzyme behave similarly and have the same excited state,[12] we have focused our present efforts on the L28F E:THF:NADPH complex, as previous backbone relaxation dispersion experiments showed that the exchange processes occur on a more favorable time scale for analysis. The present experiments yield detailed insights into the structure of the transient excited state responsible for accelerated product release, providing the first direct evidence that the product remains bound to the enzyme through its pABG tail while the pterin is displaced from the active site due to steric clash with the nicotinamide ring of the cofactor. Given the high sensitivity of proton chemical shifts to local structure, we anticipate that integrative analysis of proton side-chain relaxation dispersion experiments will emerge as an important method for probing the conformation of ligands in protein excited states.

MATERIALS AND METHODS

General Procedures. Reduced *β*-nicotinamide adenine dinucleotide phosphate tetrasodium salt hydrate (NADPH), D-glucose-6-phosphate sodium salt, and glucose-6-phosphate dehydrogenase from *Leuconostoc mesenteroides* were purchased from Sigma-Aldrich. (6*S*)-5,6,7,8-Tetrahydrofolic acid (THF) was obtained from Schircks Laboratories. Expression and purification of L28F DHFR were performed as described previously.[6,26] Isotopically labeled L28F DHFR for proton relaxation dispersion measurements was expressed in M9 medium containing 0.5 g/L of $^{15}NH_4Cl$, 0.5 g/L $^{15}NH_4(SO_4)_2$, and 3 g/L [^{13}C,^{1}H]-glucose in 99% D_2O according to published protocols.[27,28]

X-ray Crystallography. The L28F E:NADPH complex was crystallized from solutions containing 1 mM L28F DHFR, 3 mM ddTHF, 3 mM $NADP^+$, and 10 mM imidazole (pH 7.0). Crystals were grown in an anaerobic environment (NEXUS glovebox from Vacuum Atmospheres) by hanging drop vapor diffusion using a well solution containing 100 mM imidazole pH 8.0, 25% w/v PEG6000, and 450 mM $CaCl_2$. Crystals were grown at 298 K and appeared within 7 days. The L28F E:NADPH crystals were cryoprotected by soaking in well solution supplemented with 30% ethylene glycol. Diffraction data were collected at the Berkeley Center for Structural Biology beamline ALS 5.0.3. Data collection and processing statistics are summarized in Table S1. Data sets were indexed, integrated, and scaled using the HKL-2000 package.[29] The structures were solved by molecular replacement using PHASER[30] with a previously published DHFR structure (PDB code 1RX1[23]) as a search model and further refined using phenix.refine[31] combined with manual building cycles in Coot.[32] The crystallographic information file for the L28F E:NADPH structure is included in the Supporting Information. The coordinates have been deposited in the Protein Data Bank under accession number 5W3Q.

NMR Spectroscopy. Samples for CPMG relaxation dispersion NMR experiments contained 0.5 mM ^{15}N,^{13}C-labeled and partially deuterated L28F, 18 mM THF, 10 mM NADPH, 5 mM ascorbic acid, 10 mM glucose-6-phosphate, 20 units/mL glucose-6-phosphate dehydrogenase, 1 mM dithiothreitol (DTT), 25 mM KCl, and 10% D_2O in 70 mM potassium phosphate, pH 7.6. The glucose-6-phosphate recycling system was used to maintain NADPH in the reduced state.[4] Buffers were thoroughly degassed through freeze–

DOI: 10.1021/jacs.7b05958
J. Am. Chem. Soc. 2017, 139, 11233–11240

pump−thaw cycles prior to addition of ascorbic acid as an oxygen scavenger. All samples were prepared under an argon atmosphere in a glovebox, placed into amber NMR tubes, and flame-sealed.

Constant-time $^{1}H-^{13}C$ HSQC spectra were acquired on a Bruker Avance spectrometer operating at 800 MHz. Methyl assignments were transferred from the wild-type (WT) E:THF:NADPH and E:NADPH spectra.[33] ^{1}H side-chain CPMG relaxation dispersion data[28] were acquired for the L28F E:THF:NADPH complex at 500 MHz (two data sets: 16 and 32 scans) and 800 MHz (16 scans) using optimized Poisson-gap nonuniform sampling (NUS) in the indirect dimension.[34] Increased NUS sampling resolution in the time-domain was achieved by utilizing a large spectral width (140 ppm). Simulations show that increased sampling resolution improves the accuracy of peak intensity reconstruction (Figure S1). 10% of 700 real and imaginary points was acquired to maintain a high spectral resolution over the large spectral width (700 points/140 ppm) and to allow a higher number of transients to be collected in given time to obtain a greater signal-to-noise. The total relaxation time in the CPMG experiment was 40 ms. Relaxation dispersion data were processed and reconstructed using MDDNMR,[34−36] NMRpipe,[37] and FuDA (http://pound.med.utoronto.ca), and were fitted to the Bloch−McConnell equations[38] for two-site exchange using the program GLOVE.[39] Errors were set to 5% and 10% for the 800 and 500 MHz data points, respectively, unless the estimated error based on three repeat experiments was larger. Global exchange rates and minor state populations were determined by simultaneously fitting a subset of ^{1}H dispersion curves [for probes 7Hβ, 26Hβ, 50Hδ^{1}, 50Hγ^{2}, 94Hδ^{1}, 115Hδ^{1}, and 123Hγ^{2}] that were well-defined and could be fitted to a two-site exchange model. For each of these residues, the χ^{2} value for the global fit was <2 times larger than for the individual fit. All remaining dispersion curves were force-fitted, using the rates and populations for each complex determined from the global fits. It was clear from this procedure that the dispersion profiles for two methyls, A9 Hβ and V13 Hγ^{2}, reflect a small contribution from an additional exchange process and are not well fit by a two-site exchange model. These methyls, which are spatially proximal and are located ∼20 Å from the product binding pocket, were excluded from further analysis. Uncertainties in the fitted exchange parameters were estimated using Monte Carlo simulations.

Chemical Shift Predictions. Side-chain proton chemical shifts are extremely sensitive to ring currents associated with neighboring aromatic amino acids. To aid in interpretation of the relaxation dispersion data, ring current contributions to methyl proton chemical shifts for the L28F E:THF:NADPH and E:NADPH complexes were calculated from the X-ray coordinates aromatic using the program SHIFTS.[40]

RESULTS

Ground-State Structure of the L28F E:THF:NADPH Complex. The E:THF:NADPH complex is of limited stability, and the ground-state structure was therefore modeled, as in previous work with wild-type DHFR,[4,23,41] using the crystal structure of L28F E:ddTHF:NADP^{+} (PDB code 5CC9[12]), where ddTHF (5,10-dideazatetrahydrofolate) is a stable THF analogue. The E:THF:NADPH and E:THF:NADP^{+} complexes adopt nearly identical ground-state structures,[4] with the active site loops in the occluded conformation and with the nicotinamide ring of the cofactor projecting into solvent.

Structure of the L28F E:NADPH Complex. Previous ^{15}N relaxation dispersion experiments showed that the L28F E:THF:NADPH complex transiently samples a closed excited state with a backbone conformation that closely resembles the binary L28F E:NADPH complex.[12] To obtain deeper insights into the structural changes involved, we determined the crystal structure at 1.4 Å of the L28F E:NADPH complex, which was crystallized under anaerobic conditions to prevent NADPH oxidation. The backbone conformations of the closed L28F and WT E:NADPH complexes (PDB code 1RX1[23]) are very similar

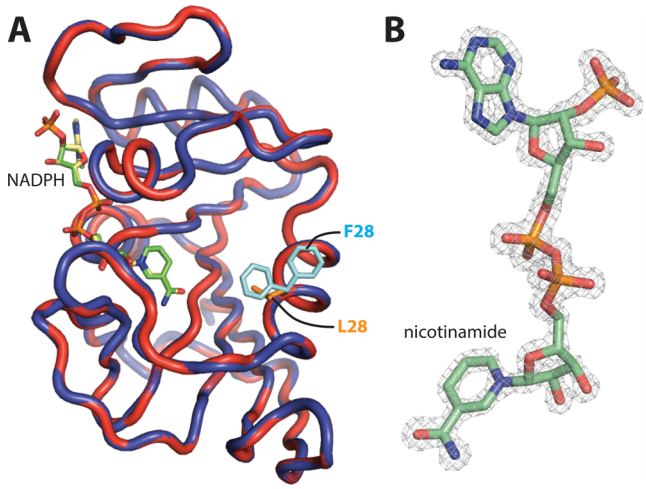

Figure 2. (A) Cartoon representation of L28F DHFR (blue) in complex with NADPH (green) superimposed on the structure of WT DHFR (red, PDB code 1RX1) in complex with NADPH (yellow). Both structures are in the closed state. Note that the NADPH molecules in the two structures are almost exactly superimposed and are difficult to distinguish in the figure. Side chains for the mutation site are shown in sticks, with the two alternative conformations observed for the F28 ring shown. (B) $2F_o - F_c$ map contoured at 2.0σ for NADPH in the L28F E:NADPH crystal structure.

(Figure 2A), with an average RMSD of 0.22 Å for the C_α atoms. The full occupancy of the ribose-nicotinamide moiety of NADPH in the L28F DHFR active site and the low Met20 loop *B*-values confirm that the cofactor remains reduced under the cryogenic conditions used to determine the structure of the L28F E:NADPH complex.

Relaxation Dispersion Experiments. To obtain insights into the structure of the excited state of the L28F E:THF:NADPH complex, we acquired side-chain proton CPMG dispersion data.[28] Relaxation dispersion was observed for many methyl groups, most of which are clustered around the active site (Figure 3A). CPMG relaxation dispersion experiments probe exchange on a microsecond−millisecond time scale between a ground state and one or more transiently populated excited-state conformations. The effective R_2 relaxation rates at two magnetic field strengths were plotted as a function of pulsing frequency (Figures 3B and S2) and fitted by the Bloch−McConnell equations.[38] For simple two-site exchange between a ground state (A) and a transient state (B), these fits yield the exchange rate constants k_a and k_b, as well as the relative populations of the two states, p_a and p_b, and the chemical shift difference ($\Delta\varpi$, in ppm[42]) between the ground and excited states. Because of the limited lifetime of the NMR samples, only the dispersion data of the methyl protons were of sufficient quality for analysis. The majority of the methyl ^{1}H dispersion curves could be fitted to a global two-site exchange model. A small number of methyl groups reflect multistate exchange, the analysis of which is beyond the scope of this work. The fitted rate and populations are very close to those determined on the basis of ^{1}H and ^{15}N backbone relaxation dispersion data (Table 1).[12] Differences are most likely due to small differences in sample preparation (including extent of deuteration) and sample heating by the CPMG pulse train.

To gain insights into the structure of the transiently populated state, we compared the methyl ^{1}H chemical shift

DOI: 10.1021/jacs.7b05958
J. Am. Chem. Soc. 2017, 139, 11233−11240

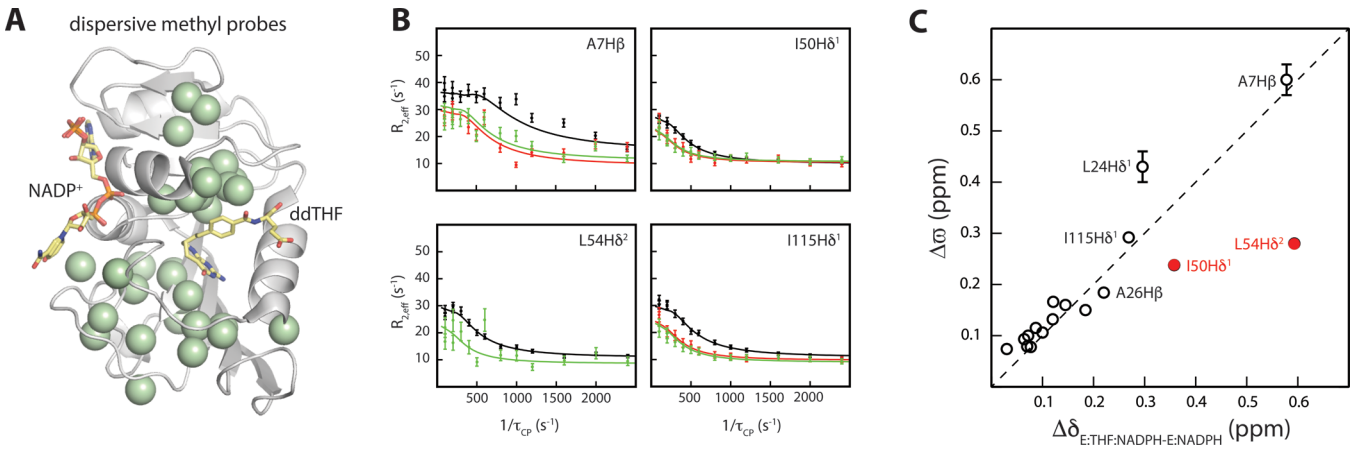

Figure 3. (A) Methyl probes that undergo ^{1}H relaxation dispersion are represented by green spheres on the L28F E:ddTHF:NADP^{+} structure, which is an analogue for the L28F E:THF:NADPH structure. (B) Representative relaxation dispersion curves for a subset of proton methyl probes; 500 MHz data acquired with 16 scans per increment (red), 500 MHz data acquired with 32 scans per increment (green), and 800 MHz data acquired with 16 scans per increment (black). (C) Correlation plot for the dynamic chemical shift differences $\Delta\varpi$ versus the static chemical shift differences, $\Delta\delta = \delta$ (E:THF:NADPH) $- \delta$ (E:NADPH). The dashed line indicates a slope = 1. Linear regression yields a slope = 1.09 and $R^2 = 0.93$, if I50Hδ^1 and L54Hδ^2 are excluded.

Table 1. Fitted Exchange Parameters

L28F E:THF:NADPH	k_{ex} (s^{-1})	p_b (%)
backbone CPMG	770 ± 20	2.75 ± 0.04
proton methyl CPMG	660 ± 40	3.54 ± 0.01

differences between the ground and excited states ($\Delta\varpi$) with the equilibrium chemical shift differences ($\Delta\delta$) between the L28F E:THF:NADPH and E:NADPH complexes. Visual inspection of the scatter plot (Figure 3C) reveals a strong correlation between $\Delta\varpi$ and $\Delta\delta$ for all methyl protons in the active site with the exception of Leu24 Hδ^1, Ile50 Hδ^1, and Leu54 Hδ^2. The uncertainty on the Leu24 Hδ^1 $\Delta\varpi$ is relatively high because only one of the three recorded data sets yielded a dispersion curve of acceptable quality (Figure S2). Excluding Ile50 and Leu54 from the linear least-squares fit yields a slope of 1.09 and R^2 of 0.93. This confirms that the process that gives rise to relaxation dispersion involves conformational exchange between the occluded ground state of the L28F E:THF:NADPH complex, with the nicotinamide ring projecting into solvent, and a weakly populated state that resembles the closed L28F E:NADPH complex.[12] The poor correlation for the Ile50 Hδ^1 and Leu54 Hδ^2 methyls is notable because of the location of these residues in the product binding pocket and will be discussed in detail below.

Sample stability is a known issue for the E:THF:NADPH complexes, and the lifetime of each sample is limited by NADPH oxidation. It was therefore of utmost importance to ensure that NADPH remains reduced during the course of our experiments, and this was accomplished by use of a glucose-6-phosphate dehydrogenase enzymatic recycling system. The sensitivity of methyl protons to ring current effects can be used to identify oxidation of NADPH to NADP^{+}. In contrast to NADP^{+}, the reduced nicotinamide ring is not aromatic and hence will not perturb nearby methyl protons through ring current effects. The Ile14 H δ^1 chemical shift is a highly sensitive probe of cofactor oxidation because it packs directly against the nicotinamide ring when the latter enters the active site pocket. When docked in the active site, the oxidized nicotinamide ring of NADP^{+} causes a predicted ring current shift of ~0.7 ppm for the Ile14 δ^1 methyl protons. However, if the nicotinamide ring is in the reduced, nonaromatic state, then transient entry into the active site in the excited state should not perturb the Ile14 H δ^1 chemical shift and should not cause dispersion for the Ile14 δ^1 methyl resonance. The complete lack of Ile14 δ^1 methyl proton dispersion (Figure S2) provides direct confirmation that the nicotinamide ring remained reduced throughout the relaxation dispersion experiment.

Backbone amide ^{15}N and ^{1}H^{N} R_2 relaxation dispersion measurements for the L28F E:THF:NADPH and E:THF:NADP^{+} complexes have been reported previously.[12] The relaxation dispersion profiles for Ala6, Ala7, Leu8, and Gly15 report on exchange processes that modulate backbone hydrogen-bonding interactions with the pterin ring of the THF product and with the nicotinamide ring of the cofactor.[25,41] The ^{15}N and ^{1}H^{N} dispersion profiles for Ala6 and the $\Delta\varpi$ values obtained from a global two-state fit of the data are shown in Figure S3.

DISCUSSION

Ground-State Structure of the L28F E:THF:NADPH Product Release Complex. Because the sensitivity of ligands to light and oxygen makes the L28F E:THF:NADPH complex a challenging target for crystallization and crystal structure determination, the ground-state structure was modeled using the complex formed by the stable product analogue 5,10-dideazatetrahydrofolate (ddTHF) and the oxidized cofactor NADP^{+}.[23] Although the crystal structures of the WT E:ddTHF:NADP^{+} (PDB code 5CCC) and L28F E:ddTHF:NADP^{+} (PDB code 5CC9) complexes are overall very similar, the benzoyl ring of the *p*-amino-benzoyl glutamate tail of ddTHF in the L28F structure is rotated 55° about its axis as compared to the corresponding wild-type complex.[12] If the differences in benzoyl orientation observed in the crystal were to persist in solution, then the methyl groups in the vicinity of the product-binding site would experience very different ring current contributions (by as much as 0.5 ppm). However, our NMR data show that methyl proton chemical shift differences between the WT and L28F E:THF:NADPH complexes are smaller than 0.05 ppm (Figure S4), indicating that the ground-

DOI: 10.1021/jacs.7b05958
J. Am. Chem. Soc. 2017, 139, 11233−11240

state structures are nearly identical and that the benzoyl rings adopt the same time-averaged orientation in solution.

Structure of the Excited State of the L28F E:THF:NADPH Complex. Previous analysis of amide ^{15}N and ^{1}H R_2 relaxation dispersion data for the WT and L28F E:THF:NADPH complexes revealed transient sampling of a closed higher-energy excited state with a backbone conformation that closely resembles that of the corresponding binary E:NADPH complexes.[12] The amide ^{15}N and ^{1}H chemical shifts of Ala7, Leu8, and Gly15 are highly sensitive to critical hydrogen-bonding interactions between the protein backbone and the nicotinamide ring and therefore report on active site occupancy by the cofactor.[25,41] The large values of $|\Delta\varpi_N|$ for Leu8 (2.80 ppm) and Gly15 (1.39 ppm) and of $|\Delta\varpi_H|$ for Ala7 (1.42 ppm), reported in ref 12, confirm that in the excited state, the nicotinamide transiently enters the active site where its carboxamide group hydrogen bonds to the backbone amide of Ala7 and the carbonyl oxygens of Ala7 and Ile14.[12,43]

The methyl proton relaxation dispersion data for the L28F E:THF:NADPH reported here provide additional evidence that the 3D structure of the transiently populated excited state is very similar to that of the closed L28F E:NADPH binary complex. Although the side-chain ^{1}H CPMG dispersion experiments allow extraction of dispersion profiles for many side-chain protons, the short lifetime of the L28F E:THF:NADPH sample limited our analysis to methyl protons, which give rise to strong cross peaks in the spectrum and high-quality dispersion data. The dispersion profiles for methyl protons, with the exception of those associated with multisite exchange clusters, were fitted globally to a two-site exchange model with similar exchange parameters as were used to fit the previously published backbone ^{15}N and ^{1}H dispersion (Table 1). Furthermore, the $\Delta\varpi$ values for the majority of methyl groups correlate with the equilibrium methyl proton chemical shift differences ($\Delta\delta$) obtained from ^{1}H−^{13}C HSQC spectra for the L28F E:THF:NADPH and L28F E:NADPH complexes (Figure 3C). This correlation shows that the methyl protons in the E:THF:NADPH excited state, which is formed by transient entry of the reduced nicotinamide ring of NADPH into the active site, experience a local environment that is very similar to that in the ground state of the closed E:NADPH complex.

Product Remains Bound in the Excited State. On the basis of considerations of the binding kinetics and the fact that the exchange rate and excited-state population are independent of THF concentration, we have argued previously that the product remains bound to the enzyme when the nicotinamide ring transiently enters the active site of the WT and L28F E:THF:NADPH complexes.[4,12] Importantly, the relaxation dispersion data presented here provide direct proof that the THF remains bound and provide detailed insights into its binding mode. Proton chemical shifts are extremely sensitive to changes in ring currents and can, therefore, be used to track the position of an aromatic ring of a ligand within its binding pocket. The product tetrahydrofolate contains two aromatic rings, one in the *N*-(*p*-aminobenzoyl)-L-glutamate (pABG) tail and one in the pterin ring system (Figure 1B). There are three methyl groups in the vicinity of these two rings: Ala7 CβH$_3$ faces the pterin ring and Ile50 Cδ^1H$_3$ and Leu54 Cδ^2H$_3$ face the benzoyl ring (Figure 4A).

The backbone ^{15}N and methyl proton chemical shifts for Ala6 and Ala7 report directly on active site occupancy by the THF pterin ring. The large value of $\Delta\varpi$ for Ala7 Hβ (0.60 ppm) correlates well with the equilibrium chemical shift

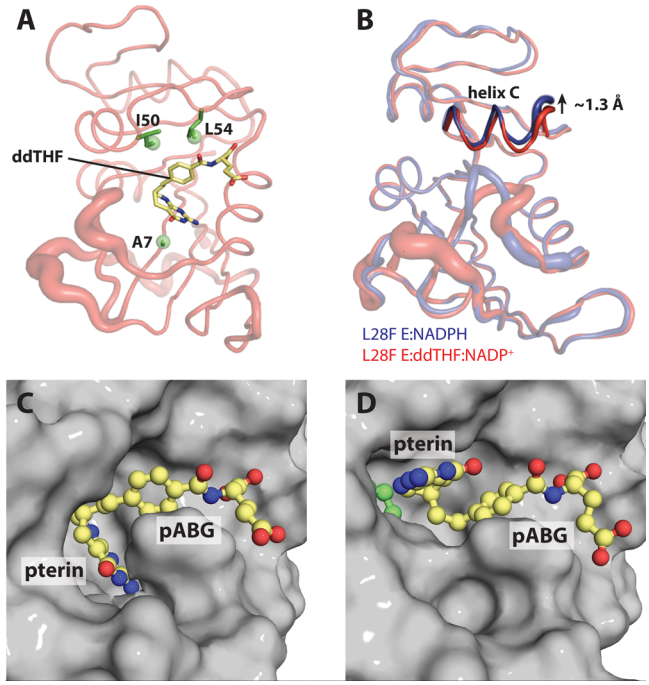

Figure 4. (A) Cartoon backbone representation of the L28F E:ddTHF:NADP$^+$ crystal structure (PDB code 5CC9). NADP$^+$ is omitted for clarity. The thickness of the loops is scaled by the *B*-value. The product analogue (ddTHF) is highlighted in yellow, residues that report on the conformation of the product in the excited state are shown as green sticks, and their specific methyl probes that undergo dispersion are shown as green spheres (A7 Hβ, I50 Hδ^1, and L54 Hδ^2). (B) Overlay of the L28F E:NADPH (blue) and L28F E:ddTHF:NADP$^+$(pink, PDB code 5CC9) crystal structures. The ligands are omitted for clarity. The thickness of the cartoon representation is scaled by the *B*-value. Helix C, which defines the upper edge of the product binding site, is shifted by 1.3 Å upward in the L28F E:NADPH structure relative to its position in the E:ddTHF:NADP$^+$ structure. The structures shown in panels A and B are rotated by 90° with respect to each other. (C) Surface representation of DHFR in the crystal structure of the occluded L28F E:ddTHF:NADP$^+$ complex showing the location of bound ddTHF (sticks and spheres, atom colors). The pterin ring is deeply buried in the active site (center left). (D) Model for the excited state of L28F E:THF:NADPH complex. The ddTHF is shown docked to the crystal structure of the closed L28F E:NADPH complex (gray surface). Rotation about the C10−C14 bond in the pABG tail rotates the pterin ring up and out of the active site to avoid steric clash with the nicotinamide ring of the NADPH (green).

difference ($\Delta\delta$ = 0.58 ppm) between the L28F E:THF:NADPH and L28F E:NADPH complexes. This correlation shows that the Ala7 β-methyl protons experience the same chemical and magnetic environment in the E:THF:NADPH excited state and in the E:NADPH ground state, and thus suggests that the pterin ring may be displaced from its binding pocket upon transient binding of the reduced nicotinamide moiety within the enzyme active site. Supporting evidence comes from ^{15}N relaxation dispersion. The amide ^{15}N resonance of Ala6 is shifted strongly downfield when the pterin group of THF or DHF occupies the active site due to formation of a hydrogen bond between the protonated pterin N8 atom and the Ile5 carbonyl.[25] A two-state fit, using the global exchange parameters for the L28F E:THF:NADPH complex reported in ref 12, of the backbone ^{15}N and ^{1}H relaxation dispersion data for Ala6 is shown in Figure S3. The large value

DOI: 10.1021/jacs.7b05958
J. Am. Chem. Soc. 2017, 139, 11233−11240

of $|\Delta\varpi_N|$ = 5.3 ppm is consistent with complete rupture of the pterin N8 to Ile5 carbonyl hydrogen bond in the excited state; density functional theory calculations[44] predict that loss of the hydrogen bond to the Ile5 carbonyl would result in an ∼5 ppm change in the Ala6 ^{15}N chemical shift. Given the restricted volume of the pterin binding pocket and the steric constraints imposed by active site side chains and the puckered nicotinamide ring of the reduced NADPH cofactor, it is highly unlikely that the hydrogen bond could be broken without displacement of the pterin ring from the active site. In contrast to E:THF:NADPH, the Ala6 $|\Delta\varpi_N|$ (=1.34 ppm) for the L28F E:THF:NADP$^+$ complex is greatly decreased, showing that the pterin remains in its binding pocket when the planar nicotinamide ring of the oxidized cofactor transiently enters the active site.

Together the Ala6 ^{15}N and Ala7 methyl proton relaxation dispersion data provide compelling evidence that the pterin ring of THF is displaced from the active site by transient entry of the reduced nicotinamide ring. However, analysis of dispersion data for other side chains shows that THF remains bound in the excited state through its *p*-aminobenzoyl glutamate (pABG) tail, but its conformation is altered to avoid steric clash between the puckered pterin and nicotinamide rings. The Ile50 Hδ^1 and Leu54 Hδ^2 methyl proton resonances, which report on the occupancy of the pABG binding pocket, are shifted upfield by 0.36 and 0.59 ppm, respectively, in spectra of the L28F E:THF:NADPH complex relative to those of the E:NADPH binary complex. This upfield shift arises from the ring current associated with the benzoyl moiety of THF, which packs against both methyl groups in crystal structures containing bound product or substrate analogs (Figure 4A). Ring current contributions from aromatic side chains are negligibly small (<0.1 ppm) and are identical for the L28F E:THF:NADPH and E:NADPH complexes, as indicated by ring current calculations performed using the X-ray coordinates. If the product was to dissociate completely from the L28F E:THF:NADPH complex, releasing the pABG moiety from its binding pocket, the Ile50 Hδ^1 and Leu54 Hδ^2 methyl proton resonances would be shifted downfield by 0.36 and 0.59 ppm, respectively. However, $\Delta\varpi$ values for the Ile50 Hδ^1 and Leu54 Hδ^2 methyl protons (0.24 and 0.28 ppm, respectively) determined from the proton relaxation dispersion measurements are substantially smaller, indicating that the product remains bound via its pABG tail in the E:THF:NADPH excited state, even though the pterin ring is displaced from the active site by entry of the reduced nicotinamide ring of the cofactor. On the basis of the differences between $\Delta\varpi$ and $\Delta\delta$, we estimate that the ring current shifts experienced by the Ile50 Hδ^1 and Leu54 Hδ^2 methyls ($\Delta\delta - \Delta\varpi$ = 0.12 and 0.31 ppm, respectively) in the L28F E:THF:NADPH excited state are substantially decreased, suggesting that the distance between the benzoyl ring of the pABG tail and the Ile50 and Leu54 side chains has increased. Inspection of the excited-state model, the L28F E:NADPH crystal structure, reveals a 1.3 Å shift of helix C away from the active site as compared to the L28F E:THF:NADPH analogue structure (L28F E:ddTHF:NADP$^+$, PDB code 5CC9) (Figure 4B). Thus, binding of the ribose-nicotinamide moiety in the active site causes the product binding site to open, which likely explains the diminished ring current shifts experienced by the Ile50 Hδ^1 and Leu54 Hδ^2 methyl groups in the excited state.

Molecular Mechanism of Allosteric Product Release. Taken together, the relaxation dispersion data show that the transient excited state of the L28F E:THF:NADPH complex has a backbone conformation that is very similar, if not identical, to the ground-state conformation of the binary E:NADPH complex.[12] Upon entry into the active site, the reduced nicotinamide ring of NADPH displaces the pterin ring of the THF product, yet the product remains bound to the enzyme through its pABG tail. An important question is how the pterin ring is able to escape from the active site pocket during the transition from the ground to the excited state. Inspection of the crystal structures of the occluded E:THF:NADP$^+$ and closed E:NADPH complexes suggests a plausible mechanism. In the occluded state, the active site is quite open (Figure 4C), allowing the pterin ring to rotate out of its binding pocket by rotation about the C10−C14 bond in the pABG tail. Rotation of the pterin during the transition to the excited state, concomitant with binding of the reduced nicotinamide ring in the active site and closure of the Met20 loop, would place the pterin in a newly formed cleft (observed in the crystal structure of the closed L28F E:NADPH complex) between helix C and the Met20 loop, without displacing the pABG tail from its binding site. A structural model for the excited-state conformation of the THF is shown in Figure 4D. Backbone relaxation dispersion data indicate that the excited states for the L28F and WT E:THF:NADPH complexes are identical,[12] indicating that the THF most probably adopts a similar conformation in the excited state of the WT product release complex.

Rotation of the pterin ring out of the active site would disrupt an extensive network of direct and water-mediated hydrogen bonds and hydrophobic contacts and would therefore be expected to greatly diminish the THF binding affinity and enhance the rate of THF dissociation from the excited state of the E:THF:NADPH complex. Assuming that the rate of association of THF to the L28FE:NADPH complex is the same as for WT *E. coli* DHFR (k_{on} = 2 × 10^6 M^{-1} s^{-1})[22] and given the rate of THF dissociation from the excited state of L28F E:THF:NADPH measured by NMR relaxation dispersion (k_{off} = 1000 s^{-1}),[12] we estimate the K_d for binding of THF in the excited state to be ∼0.5 mM. This value is in excellent agreement with the K_d value (1 mM) measured for binding of *p*-aminobenzoyl-L-glutamate to *L. casei* DHFR,[45] suggesting that binding of THF in the excited state of the product release complex is likely dominated by interactions with the pABG moiety.

CONCLUSIONS

Cofactor-mediated product release is an important mechanism to ensure proper turnover and to avoid product inhibition. Previously, we have provided a quantitative description of the kinetics of product release. Here, we add molecular detail by establishing the structural basis for cofactor-mediated product release in the L28F mutant. Two allosteric events are responsible for the release of the product. First, transient entry of the reduced nicotinamide moiety into the active site pocket causes a steric clash with the pterin ring of the product tetrahydrofolate, facilitating release of the pterin ring from the active site. Second, transient binding of the ribose moiety causes helix C to shift, thereby opening the pABG cleft and further assisting product release. Despite these major structural perturbations, the product remains weakly bound through its pABG tail in the excited state of the L28F E:THF:NADPH complex. Thus, through entry of the nicotinamide ring into the active site, the NADPH cofactor transiently remodels the

DOI: 10.1021/jacs.7b05958
J. Am. Chem. Soc. 2017, 139, 11233−11240

enzyme structure to form a weakly populated excited state that is poised for rapid product release.

■ ASSOCIATED CONTENT

Supporting Information

The Supporting Information is available free of charge on the ACS Publications website at DOI: 10.1021/jacs.7b05958.

X-ray crystallographic data for the L28F E:NADPH structure (CIF)

Figures showing peak intensities obtained from non-uniformly sampled spectra as compared to reconstructed fully sampled data; methyl proton relaxation dispersion profiles for all residues showing two-site exchange in L28F E:THF:NADPH; backbone relaxation dispersion profiles for Ala6 in two L28F complexes; comparison of predicted and observed chemical shift differences; a table showing crystallographic data collection and refinement statistics; and a table showing values of chemical shift differences from fits of methyl proton dispersion profiles (PDF)

■ AUTHOR INFORMATION

Corresponding Author

*wright@scripps.edu

ORCID

R. Bryn Fenwick: 0000-0002-0925-7422

H. Jane Dyson: 0000-0001-6855-3398

Present Address

†Department of Pharmacology, University of California, 9500 Gilman Drive #0654, San Diego, California 92093, United States.

Notes

The authors declare no competing financial interest.

■ ACKNOWLEDGMENTS

This work was supported by the U.S. National Institutes of Health (NIH) grant GM75995 (P.E.W.) and the Skaggs Institute of Chemical Biology (P.E.W. and I.A.W.). D.O. was supported by a Collen-Francqui fellowship from the Belgian American Educational Foundation (B.A.E.F.). We thank Maria Yamout and Gerard Kroon for expert assistance with experiments. The Berkeley Center for Structural Biology is supported in part by the National Institutes of Health, National Institute of General Medical Sciences, and the Howard Hughes Medical Institute. The Advanced Light Source is a Department of Energy Office of Science User Facility under contract no. DE-AC02-05CH11231.

■ REFERENCES

(1) Eisenmesser, E. Z.; Bosco, D. A.; Akke, M.; Kern, D. *Science* **2002**, *295*, 1520.

(2) Wolf-Watz, M.; Thai, V.; Henzler-Wildman, K.; Hadjipavlou, G.; Eisenmesser, E. Z.; Kern, D. *Nat. Struct. Mol. Biol.* **2004**, *11*, 945.

(3) Eisenmesser, E. Z.; Millet, O.; Labeikovsky, W.; Korzhnev, D. M.; Wolf-Watz, M.; Bosco, D. A.; Skalicky, J. J.; Kay, L. E.; Kern, D. *Nature* **2005**, *438*, 117.

(4) Boehr, D. D.; McElheny, D.; Dyson, H. J.; Wright, P. E. *Science* **2006**, *313*, 1638.

(5) Henzler-Wildman, K. A.; Thai, V.; Lei, M.; Ott, M.; Wolf-Watz, M.; Fenn, T.; Pozharski, E.; Wilson, M. A.; Petsko, G. A.; Karplus, M.; Hubner, C. G.; Kern, D. *Nature* **2007**, *450*, 838.

(6) Bhabha, G.; Lee, J.; Ekiert, D. C.; Gam, J.; Wilson, I. A.; Dyson, H. J.; Benkovic, S. J.; Wright, P. E. *Science* **2011**, *332*, 234.

(7) Kerns, S. J.; Agafonov, R. V.; Cho, Y.-J.; Pontiggia, F.; Otten, R.; Pachov, D. V.; Kutter, S.; Phung, L. A.; Murphy, P. N.; Thai, V.; Alber, T.; Hagan, M. F.; Kern, D. *Nat. Struct. Mol. Biol.* **2015**, *22*, 124.

(8) Whittier, S. K.; Hengge, A. C.; Loria, J. P. *Science* **2013**, *341*, 899.

(9) De Simone, A.; Aprile, F. A.; Dhulesia, A.; Dobson, C. M.; Vendruscolo, M. *eLife* **2015**, *4*, 1.

(10) Kim, T. H.; Mehrabi, P.; Ren, Z.; Sljoka, A.; Ing, C.; Bezginov, A.; Ye, L.; Pomès, R.; Prosser, R. S.; Pai, E. F. *Science* **2017**, *355*, eaag2355.

(11) Peng, Y.; Hansen, A. L.; Bruschweiler-Li, L.; Davulcu, O.; Skalicky, J. J.; Chapman, M. S.; Brüschweiler, R. *J. Am. Chem. Soc.* **2017**, *139*, 4846.

(12) Oyen, D.; Fenwick, R. B.; Stanfield, R. L.; Dyson, H. J.; Wright, P. E. *J. Am. Chem. Soc.* **2015**, *137*, 9459.

(13) Boehr, D. D.; Dyson, H. J.; Wright, P. E. *Chem. Rev.* **2006**, *106*, 3055.

(14) Palmer, A. G. *Acc. Chem. Res.* **2015**, *48*, 457.

(15) Loria, J. P.; Rance, M.; Palmer, A. G., III *J. Am. Chem. Soc.* **1999**, *121*, 2331.

(16) Trott, O.; Palmer, A. G. *J. Magn. Reson.* **2002**, *154*, 157.

(17) Fawzi, N. L.; Ying, J.; Ghirlando, R.; Torchia, D. A.; Clore, G. M. *Nature* **2011**, *480*, 268.

(18) Vallurupalli, P.; Bouvignies, G.; Kay, L. E. *J. Am. Chem. Soc.* **2012**, *134*, 8148.

(19) Bouvignies, G.; Vallurupalli, P.; Hansen, D. F.; Correia, B. E.; Lange, O.; Bah, A.; Vernon, R. M.; Dahlquist, F. W.; Baker, D.; Kay, L. E. *Nature* **2011**, *477*, 111.

(20) Schnell, J. R.; Dyson, H. J.; Wright, P. E. *Annu. Rev. Biophys. Biomol. Struct.* **2004**, *33*, 119.

(21) Hammes, G. G.; Benkovic, S. J.; Hammes-Schiffer, S. *Biochemistry* **2011**, *50*, 10422.

(22) Fierke, C. A.; Johnson, K. A.; Benkovic, S. J. *Biochemistry* **1987**, *26*, 4085.

(23) Sawaya, M. R.; Kraut, J. *Biochemistry* **1997**, *36*, 586.

(24) Wishart, D. S.; Case, D. A. *Methods Enzymol.* **2001**, *338*, 3.

(25) Venkitakrishnan, R. P.; Zaborowski, E.; McElheny, D.; Benkovic, S. J.; Dyson, H. J.; Wright, P. E. *Biochemistry* **2004**, *43*, 16046.

(26) Cameron, C. E.; Benkovic, S. J. *Biochemistry* **1997**, *36*, 15792.

(27) Otten, R.; Villali, J.; Kern, D.; Mulder, F. A. A. *J. Am. Chem. Soc.* **2010**, *132*, 17004.

(28) Hansen, A. L.; Lundström, P.; Velyvis, A.; Kay, L. E. *J. Am. Chem. Soc.* **2012**, *134*, 3178.

(29) Otwinowski, Z.; Minor, W. In *Methods in Enzymology Macromolecular Crystallography, Part A*; Carter, C. W., Jr., Sweet, R. M., Eds.; Academic Press: New York, 1997; Vol. *276*, p 307.

(30) McCoy, A. J.; Grosse-Kunstleve, R. W.; Adams, P. D.; Winn, M. D.; Storoni, L. C.; Read, R. J. *J. Appl. Crystallogr.* **2007**, *40*, 658.

(31) Adams, P. D.; Afonine, P. V.; Bunkoczi, G.; Chen, V. B.; Davis, I. W.; Echols, N.; Headd, J. J.; Hung, L. W.; Kapral, G. J.; Grosse-Kunstleve, R. W.; McCoy, A. J.; Moriarty, N. W.; Oeffner, R.; Read, R. J.; Richardson, D. C.; Richardson, J. S.; Terwilliger, T. C.; Zwart, P. H. *Acta Crystallogr., Sect. D: Biol. Crystallogr.* **2010**, *66*, 213.

(32) Emsley, P.; Lohkamp, B.; Scott, W. G.; Cowtan, K. *Acta Crystallogr., Sect. D: Biol. Crystallogr.* **2010**, *66*, 486.

(33) Tuttle, L. M.; Dyson, H. J.; Wright, P. E. *Biochemistry* **2013**, *52*, 3464.

(34) Aoto, P. C.; Fenwick, R. B.; Kroon, G. J. A.; Wright, P. E. *J. Magn. Reson.* **2014**, *246*, 31.

(35) Orekhov, V. Y.; Jaravine, V. A. *Prog. Nucl. Magn. Reson. Spectrosc.* **2011**, *59*, 271.

(36) Kazimierczuk, K.; Orekhov, V. Y. *Angew. Chem., Int. Ed.* **2011**, *50*, 5556.

(37) Delaglio, F.; Grzesiek, S.; Vuister, G. W.; Guang, Z.; Pfeifer, J.; Bax, A. *J. Biomol. NMR* **1995**, *6*, 277.

(38) Palmer, A. G., III *Chem. Rev.* **2004**, *104*, 3623.

DOI: 10.1021/jacs.7b05958
J. Am. Chem. Soc. 2017, 139, 11233−11240

(39) Sugase, K.; Konuma, T.; Lansing, J. C.; Wright, P. E. *J. Biomol. NMR* **2013**, *56*, 275.
(40) Ösapay, K.; Case, D. A. *J. Am. Chem. Soc.* **1991**, *113*, 9436.
(41) Boehr, D. D.; McElheny, D.; Dyson, H. J.; Wright, P. E. *Proc. Natl. Acad. Sci. U. S. A.* **2010**, *107*, 1373.
(42) Skrynnikov, N. R.; Dahlquist, F. W.; Kay, L. E. *J. Am. Chem. Soc.* **2002**, *124*, 12352.
(43) Fenwick, R. B.; Oyen, D.; Wright, P. E. *Phys. Chem. Chem. Phys.* **2016**, *18*, 5789.
(44) Xu, X. P.; Case, D. A. *Biopolymers* **2002**, *65*, 408.
(45) Birdsall, B.; Burgen, A. S. V.; Rodrigues de Miranda, J.; Roberts, G. C. K. *Biochemistry* **1978**, *17*, 2102.

DOI: 10.1021/jacs.7b05958
J. Am. Chem. Soc. 2017, 139, 11233−11240